

# POM-1 inhibits P2 receptors and exhibits anti-inflammatory effects in macrophages

Gabriela Pimenta-dos-Reis<sup>1</sup> · Eduardo José Lopes Torres<sup>2</sup> · Paula Gabriela Quintana<sup>1</sup> · Lincon Onorio Vidal<sup>1</sup> · Bárbara Andréa Fortes dos Santos<sup>1</sup> · Chuan-Sheng Lin<sup>3,4</sup> · Norton Heise<sup>1</sup> · Pedro Muanis Persechini<sup>1</sup> · Julieta Schachter<sup>3,5</sup>

Received: 4 June 2017 / Accepted: 2 October 2017 / Published online: 11 October 2017  
© Springer Science+Business Media B.V. 2017

**Abstract** Extracellular nucleotides can modulate the immunological response by activating purinergic receptors (P2Rs) on the cell surface of macrophages, dendritic, and other immune cells. In particular, the activation of P2X7R can induce release of cytokines and cell death as well as the uptake of large molecules through the cell membrane by a mechanism still poorly understood. Polyoxotungstate-1 (POM-1) has been proposed as a potent inhibitor of ecto-nucleotidases, enzymes that hydrolyze extracellular nucleotides, regulating the activity of P2Rs. However, the potential impact of POM-1 on P2Rs has not been evaluated. Here, we used fluorescent dye uptake, cytoplasmic free  $Ca^{2+}$  concentration measurement, patch-clamp recordings, scanning electron microscopy, and quantification of inflammatory mediators to investigate the effects of POM-1 on P2Rs of murine macrophages. We ob-

served that POM-1 blocks the P2YR-dependent cytoplasmic  $Ca^{2+}$  increase and has partial effects on the cytoplasmic  $Ca^{2+}$ , increasing dependence on P2XRs. POM-1 can inhibit the events related with ATP-dependent inflammasome activation, anionic dye uptake, and also the opening of large conductance channels, which are associated with P2X7R-dependent pannexin-1 activation. On the other hand, this compound has no effects on cationic fluorescent dye uptake, apoptosis, and bleb formation, also dependent on P2X7R. Moreover, POM-1 can be considered an anti-inflammatory compound, because it prevents TNF- $\alpha$  and nitric oxide release from LPS-treated macrophages.

**Keywords** ATP · Purinergic receptor · POM-1 · Macrophage · Inflammation

✉ Julieta Schachter  
julischachter@gmail.com

Gabriela Pimenta-dos-Reis  
g.pimentareis@gmail.com

Eduardo José Lopes Torres  
eduardo.torres@uerj.br

Paula Gabriela Quintana  
pauquintana@gmail.com

Lincon Onorio Vidal  
linconvidal@gmail.com

Bárbara Andréa Fortes dos Santos  
barbarafortes@hotmail.com

Chuan-Sheng Lin  
roylin.oa@gmail.com

Norton Heise  
nheise@biof.ufrj.br

Pedro Muanis Persechini  
pedropersechini@gmail.com

- <sup>1</sup> Instituto de Biofísica Carlos Chagas Filho da Universidade Federal de Rio de Janeiro, Rio de Janeiro, Brazil
- <sup>2</sup> Laboratório de Helminologia Romero Lascasas Porto, Departamento de Microbiologia, Imunologia e Parasitologia, Faculdade de Ciências Médicas, Universidade do Estado do Rio de Janeiro, Rio de Janeiro, Brazil
- <sup>3</sup> Microbiota Research Center, Chang Gung University, Taoyuan, Taiwan
- <sup>4</sup> Center for Molecular and Clinical Immunology, Chang Gung University, Taoyuan, Taiwan
- <sup>5</sup> Polo Xerem, Universidade Federal de Rio de Janeiro, Estrada de Xerém No. 27, Xerém, Duque de Caxias, Rio de Janeiro 25245-390, Brazil

## Introduction

Extracellular ATP (eATP) and its derivatives are key mediators in the immune system, acting as pro-inflammatory or anti-inflammatory factors depending on concentration and the receptors expressed in each particular tissue [1]. Nucleotides function as immunomodulators by activation of cell surface P2 receptors (P2Rs) [2]. P2Rs fall into two classes: the ionotropic P2XRs (P2X1–7R) and the G protein-coupled P2YRs (P2Y1, 2, 4, 6, 11, 12, 13, and 14R) [3, 4]. Both types of P2Rs are expressed by macrophages, dendritic, and endothelial cells, as well as by other immune cells [5].

P2X7R is a cation-selective channel permeable to  $\text{Na}^+$ ,  $\text{K}^+$ , and  $\text{Ca}^{2+}$  and exhibits a number of unusual properties, including the ability to change membrane permeability. After prolonged exposure to millimolar concentrations of ATP, P2X7R-dependent permeabilization pathways with high conductance are opened, allowing the passage of molecules with an upper limit of approximately 900 Da in macrophages [6]. Two main hypotheses have been proposed to explain the mechanism of permeation to larger molecules: (1) dilation of the channel portion of the receptor after prolonged exposure to high agonist concentrations [7] and (2) opening of a protein pore distinct from the receptor itself [8]. It has been proposed that pannexin-1 (pnx-1) channels are the molecules responsible for P2X7R-associated pores [9]. However, recent evidence has shown that uptake process of P2X7R-associated molecules is more complicated than a single permeation pathway and presents different selectivity for cationic and anionic molecules, indicating the possible co-existence of multiple transport mechanisms [10, 11]. Recently, the possibility that the permeation of organic dyes can occur directly through the P2X7R channel without the need of either additional molecules or “pore dilation” has also been proposed [12]. New pharmacological tools are needed to better characterize these different pathways.

P2X7R activation has been widely studied as a trigger of the NLRP3 inflammasome, but eATP through P2X7R can modulate immune functions even in an inflammasome-independent manner [13]. P2X7R can induce cell death, cytokine release, killing of intracellular pathogens, and membrane blebbing [14–17]. The specific pathways that lead to each P2X7R-dependent response in immune cells are still poorly understood, as is the link between these functional responses and the change in membrane permeability.

The interplay between eATP and P2Rs is influenced by the activity of surface ecto-nucleotidases, which hydrolyze extracellular nucleotides in a stepwise manner to ADP, AMP, and adenosine. Four ecto-nucleotidase families have been described: ecto-nucleoside triphosphate diphosphohydrolases (NTPDases), ecto-5'-nucleotidase (5'-NT), ecto-nucleotide pyrophosphatases/phosphodiesterases (NPPs), and alkaline phosphatases (APs) [18]. NTPDase1/CD39 hydrolyzes

extracellular triphosphonucleosides and diphosphonucleosides to monophosphonucleosides and is the dominant ecto-nucleotidase in immune cells [19, 20]. Besides their potential role as modulators of P2Rs, ecto-nucleotidases are also involved in immunomodulation and infection [21, 22]. So, to completely define the roles that nucleotides and nucleosides play in purinergic signaling, it would be useful to prevent the extracellular metabolism of nucleotides by blocking ecto-nucleotidases. However, there are only a few potent inhibitors of these enzymes, and many of the available blockers are expensive, unstable, and/or unspecific, also inhibiting P2Rs [23, 24]. For example, suramin is a well-known and widely used generic P2R antagonist [25] and also an E-NTPDase inhibitor, as are PPADS [26] and BG0 [27].

Polyoxometalates (POMs) are negatively charged inorganic compounds that contain metal ions surrounded by oxygen atoms [28]. Because these compounds have high molecular weights and are not drug-like molecules, they were found to be useful pharmacological tools [23, 29, 30]. Sodium polyoxotungstate (POM-1) was proposed as a potent inhibitor of NTPDase1, 2, and 3 [31], and since then, it has been used in different models. POMs have been shown to exhibit biological activities, including anticancer [32], antibacterial [33], antiprotozoal [34], antiviral [22, 35], and antidiabetic activities [36]. However, their biological mechanisms of action at the molecular level are not well understood.

In particular, the potential effects of POM-1 on purinergic receptors have not been evaluated, even when this compound has been used in P2R studies [37–39]. In the present study, we investigated the effects of POM-1 on P2R signaling, with focus on P2X7R and its pro-inflammatory activity in murine macrophages. To evaluate the different phenomena associated with P2Rs, we used fluorescent dye uptake, cytoplasmic free  $\text{Ca}^{2+}$  concentration measurement with Fura-2, patch-clamp recordings, scanning electron microscopy, and quantification of inflammatory mediators, such as pro-inflammatory cytokines and nitric oxide (NO). We conclude that POM-1 has inhibitory action on P2YR-dependent cytoplasmic  $\text{Ca}^{2+}$  increase and some but not all P2X7R-associated responses. Additionally, POM-1 can be considered an anti-inflammatory compound, because it prevents  $\text{TNF-}\alpha$  and NO release from LPS-treated macrophages.

## Material and methods

### Material

Dulbecco's modified Eagle's medium (DMEM), fetal bovine serum, penicillin, and streptomycin were obtained from Gibco (São Paulo, SP, Brazil); thioglycollate medium was acquired from Difco (Detroit, MI, USA); NaCl and  $\text{MgCl}_2$  were purchased from Vetec (Rio de Janeiro, RJ, Brazil); KCl and

ethanol were obtained from Reagen (Rio de Janeiro, RJ, Brazil);  $K_3Fe(CN)_6$ ,  $CaCl_2$ , EGTA, HEPES, dimethylsulfoxide (DMSO), carboxyfluorescein (CF), ionomycin, probenecid, phosphate-buffered saline (PBS), sulforhodamine B (SR-B), adenosine triphosphate (ATP), adenosine diphosphate (ADP), adenosine monophosphate (AMP), uridine triphosphate (UTP), sodium polyoxotungstate (POM-1), sodium molybdate, malachite green, Triton X-100, ethidium bromide (EB), and LPS from *Escherichia coli* 0111:B4 were purchased from Sigma-Aldrich (São Paulo, SP, Brazil); Fura-2 AM came from Life Technologies (São Paulo, SP, Brazil), and BAPTA-AM was obtained from Invitrogen (São Paulo, SP, Brazil).

### Animals

Swiss-Webster mice were obtained from the animal facilities of the Centro de Criação de Animais de Laboratório (CECAL), FIOCRUZ (Rio de Janeiro, RJ, Brazil). All animals were 8 to 12 weeks old, weighed approximately 16–25 g, and were handled according to the guidelines for animal use in scientific experiments of the Carlos Chagas Filho Institute of Biophysics of Federal University of Rio de Janeiro. The protocols were approved by the Research Ethics Committee on Animal Care of the Health Science Center of Federal University of Rio de Janeiro (protocol number 001200.001568/2013-87).

### Macrophage isolation and culture

Thioglycollate-elicited macrophages were obtained from the intraperitoneal cavity of mice, 4 days after thioglycollate injection, as previously described [10]. Briefly, cells were washed in DMEM and plated on 35-mm culture dishes, 12, 24, or 96-well plates or glass coverslips, according to the experiment. The cultures were maintained in DMEM supplemented with 10% fetal bovine serum, 2 g/L sodium bicarbonate, 0.3 mg/L L-glutamine, 100 U/mL penicillin, and 100 µg/mL streptomycin (supplemented medium) at 37 °C in a humidified atmosphere containing 5%  $CO_2$ . Non-adherent cells were removed after 40 min, and the macrophages were kept for 4 days under the same culture conditions.

### Ecto-nucleotidase activity assays

Ecto-nucleotidase activity was determined using the malachite green assay and high-performance liquid chromatography (HPLC). Using the malachite green colorimetric assay, NTPDase activity in macrophages ( $2 \times 10^5$  cells/petri dish) was determined by measuring the amount of liberated inorganic phosphate (Pi) [40]. Prior to testing, the cells were washed with reaction medium containing (in mM) 1  $CaCl_2$ , 145 NaCl, 5 KCl, 10 HEPES, and 1  $MgCl_2$  at pH 7.4 (normal

saline solution). The reaction was initiated by adding the nucleotide substrate to the culture dish and stopped by the addition of the supernatants of the cultures in a tube containing 1 mL of cold 25% charcoal in 0.1 M HCl. This charcoal suspension was washed at least 20 times with 0.1 M HCl before use to avoid inorganic phosphate (Pi) contamination [41]. The tubes were centrifuged at  $1500 \times g$  for 10 min. Aliquots (50 µL) of the supernatants containing the released Pi were quantified using the malachite green colorimetric reagent and a solution containing different concentrations of Pi as standard. The malachite green reagent was prepared by mixing 2 g of sodium molybdate, 0.3 g of malachite green, and 0.5 g of Triton X-100 in 1 L of 0.7 M HCl. Controls to determine non-enzymatic Pi release were performed by incubating the cells in the absence of substrate or incubating the substrate in the absence of cells, which were added after the reaction was stopped.

For the HPLC-UV analysis, macrophages ( $2 \times 10^6$  cells/petri dish) cultured as described above were incubated with 3 mM ATP for 30 min with or without 100 µM POM-1 in normal saline solution. The supernatants were collected; the pH was adjusted to 6.5 with 3.5 M NaOH/1 M  $HCO_3^-$ , and the samples were centrifuged for 10 min at  $15,000 \times g$ . The supernatant was analyzed with a Prominence HPLC (Shimadzu, Japan), equipped with a vacuum degasser, a binary pump with a manual injector, and UV detector. Nucleosides were separated at room temperature in a C-18 Kromasil column ( $250 \times 4.6$  mm) using 1 mL/min flow rate of 100 mM  $H_3PO_4$  pH 6.2 adjusted with TEA (mobile phase A) and 5 mM solution of  $MgSO_4$  in the mobile phase A (mobile phase B). The elution program was composed of 3% B (0–5 min) followed by a linear gradient of 3 to 100% B (5–38 min) and 100% B (38–90 min). Peaks were detected at 254 nm, identified by their retention times, and confirmed after co-injection of each supernatant spiked with authentic standards. Calibration curves were assessed by the integration of peaks of each standard (prepared as 2 mM stock solutions in PBS) in the range of 1 µM and 1 mM ( $r^2 > 0.9982$ ).

### Intracellular calcium measurements

Macrophages ( $2 \times 10^5$  plated on glass coverslips) were loaded with 5 µM Fura-2 AM at 37 °C in supplemented medium containing 2.5 mM probenecid during 40 min. The cells were then washed twice in normal saline solution and placed in a chamber whose base was formed by the coverslip containing the cells. The cells were maintained at 37 °C or room temperature (depending of the experiment) in normal saline solution. Cytoplasmic calcium concentrations of groups of 20–30 cells were monitored continuously with the use of a fluorescence imaging spectrofluorimeter (Easy Ratio Pro) equipped with a DeltaRAMX Illuminator, an Olympus IX71 microscope, a QuantEM 5125C camera, and the ImagePro Plus V 6.3

software (PTI Photon Technology International, Princeton, NJ, USA) at 37 °C or room temperature. Fura-2 was excited alternately at 340 and 380 nm, and the emission at 510 nm was measured. The ratio measurement is proportional to the cytoplasmic calcium concentration and was determined every 100 ms. Nucleotide application was performed by gently adding 20  $\mu$ L of the appropriate concentration nucleotide solution with a manual pipette. Maximum and minimum fluorescence values were obtained by adding ionomycin (20  $\mu$ M) and EGTA (10 mM), respectively.

### Dye uptake

Unless otherwise specified, macrophages ( $1 \times 10^5$ ) were kept at 37 °C for 5 min, in normal saline solution before the experiment. The fluorescent dyes CF (5 mM) or SR-B (200  $\mu$ M) and ATP (5 mM) were then added, and the cells were kept under the same conditions for an additional period of 10 min. In some experiments, cells were pre-incubated with POM-1 for a period of 30 min, as specified in the figure legends. Dye uptake was then determined either by fluorescence microscopy or by quantitative spectrofluorimetry, as described below.

Fluorescence microscopy was performed using an Axiovert 100 microscope (Karl Zeiss, Oberkochen, Germany) equipped with an HBO lamp, a digital camera (Olympus American Inc., PA, USA), and Image-Pro Plus v6.2 software (Media Cybernetics, Inc., Bethesda, MD, USA).

Quantitative spectrofluorimetry was performed in experiments with CF or SR-B, using an FLX-800 plate reader (BioTek Instruments Inc., Winooski, VT, USA) according to the following protocol. The cells were gently washed five times with PBS, lysed by the addition of 100  $\mu$ L PBS containing 0.01% BSA and 0.1% Triton X-100, and scraped off the plate, and the content was employed for fluorescence determination using the following excitation and emission wavelength ranges (nm): 420–450 and 528–520 for CF and 516–520 and 620–640 for SR-B. Protein concentrations were determined by the Bradford method.

### Electrophysiological measurements

Macrophages ( $1 \times 10^5$ ) were plated in 35-mm plastic culture dishes for 3 days in the conditions described above. Before the experiment, the culture medium was exchanged for normal saline solution (see below). Experiments were performed at  $-40$  mV holding potential, maintaining the cells at 37 °C using a heating chamber. Ionic currents were recorded in whole-cell or cell-attached configurations, using an Axonpatch 200B amplifier (Axon Instruments, USA) according to standard patch-clamping techniques [42]. High-resistance seals (1–5 G $\Omega$ ) were formed after offset potential compensation, using micropipettes filled with a solution

containing (in mM) 135 KCl, 5 NaCl, 2 MgCl<sub>2</sub>, 0.1 EGTA, and 10 HEPES, pH 7.4, in the whole-cell experiments, and normal saline solution in cell-attached experiments. ATP at the indicated concentrations was applied to the cell cultures by pneumatic injection, using a pneumatic pump (NeuroPhore BH-2 system, Harvard Apparatus, USA). Data were collected using pClamp software, version 10.2, and a Digidata 1140 interface (Axon Instruments, USA) and plotted using GraphPad Prism software, version 6.0 (USA).

### Induction and analysis of cell death

**Apoptosis induction** Macrophages ( $2 \times 10^5$ /well plated in 12-well culture plates) were pre-incubated at 37 °C with or without POM-1 for 30 min in DMEM and then with or without 5 mM ATP for an additional 30 min. After this period, cells were gently washed twice and incubated for 6 h at 37 °C with supplemented DMEM. The cells were then centrifuged at 5600 $\times$ g for 1 min, and the pellet was used for determination of apoptosis, as described in [43, 44]. Briefly, the cells were suspended in 250  $\mu$ L of a lysing buffer that preserved the nuclei for the determination of DNA content (50  $\mu$ g/mL EB, 0.1% sodium citrate, 0.1% Triton X-100). The nuclei were then analyzed by flow cytometry (FACSCalibur, Becton Dickinson, Mountain View, USA), and the degree of apoptosis was quantified by counting the number of hypodiploid events. At least 3000 events were collected per sample, and normalized values were calculated by subtracting the spontaneous apoptosis obtained in the controls (absence of any treatment) from all experimental values and calculating the percent of the number of hypodiploid events (percent of apoptosis) induced by 5 mM ATP as 100%.

**Pyroptosis induction** Macrophages ( $5 \times 10^6$ /well plated in a 24-well plate) were washed two times and then pre-incubated with POM-1 for 30 min in supplemented DMEM at 37 °C. After that, the cells were treated with LPS (100 ng/mL) for 6 h, finally adding ATP (3 mM) for 2 h in the same conditions. Macrophages were also treated only with POM-1 for 8 h, ATP for 2 h, or LPS for 6 h. After this period, the cells were centrifuged at 5600 $\times$ g for 1 min, and the supernatant was collected to measure the lactate dehydrogenase (LDH) content. The LDH enzymatic activity in the supernatants was determined by using a commercially available colorimetric assay kit according to the maker's instructions (Dolex, Goiania, GO, Brazil). Controls were obtained by using supernatants of untreated cells (0%) and cells treated with 1% saponin for 30 min (100%). Each reading was subtracted from the reading obtained in medium containing POM-1 without cells in order to avoid any possible interference of this compound with the reagents in the LDH detection kit.



## Light and scanning electron microscopy

For light microscopy, images of macrophages ( $1 \times 10^5$  per coverslip) were obtained using a differential interference contrast (DIC) system in an Olympus BX 51 microscope with Olympus DP-12 digital camera.

For scanning electron microscopy (SEM), cells adhered in glass coverslips were fixed in solution that consisted of 2.5% glutaraldehyde in 0.1 M cacodylate buffer, pH 7.2. Cells were fixed for 1 h at room temperature and 12 h at 4 °C. After this period, the samples were washed in 0.1 M cacodylate buffer, post-fixed in 1% OsO<sub>4</sub> and 0.8% K<sub>3</sub>Fe(CN)<sub>6</sub>, washed in distilled water, dehydrated in a graded ethanol series (20 GL absolute) for 20 min each step, critical point dried in liquid CO<sub>2</sub>, mounted on metallic stubs, and coated with gold (20–25 nm deposited). The samples were examined using an FEI Quanta 250 scanning electron microscope operating at 25–30 kV, in high vacuum mode.

## IL-1 $\beta$ and TNF- $\alpha$ release assays

Macrophages ( $5 \times 10^6$ /well plated in a 24-well plate) were washed two times and then pre-incubated with POM-1 for 30 min in supplemented DMEM at 37 °C. After that, the cells were treated with LPS (100 ng/mL) for 6 h, finally adding ATP (3 mM) for 2 h in the same conditions. The supernatant was collected, and the amounts of IL-1 $\beta$  and TNF- $\alpha$  were measured by ELISA kit (PeproTech, USA) according to the manufacturer's manual. Assays were performed in duplicate for each independent experiment.

## Nitric oxide assay

Macrophages ( $5 \times 10^5$ /well plated in 96-well plates) were treated or not with LPS (at the concentrations indicated) for 24 h, with or without of 100  $\mu$ M POM-1. After this time, the culture supernatants were collected for measurement of the amount of nitrite using the Griess colorimetric method [45]. In this method, nitrite reacts with sulfanilamide and *N*- $\alpha$ -naphthyl-ethylenediamine, giving a coloration that can be evaluated using an ELISA microplate reader with a filter for a wavelength of 550 nm.

## Data analysis

Differences between experimental groups were evaluated by the Mann-Whitney non-parametric test. Data were analyzed using GraphPad Instat software (GraphPad Software Inc., v5.0).

## Results

### Ecto-nucleotidase activity in macrophage is inhibited by POM-1

To characterize the ecto-nucleotidase activity on the surface of murine macrophages, we incubated the cells with 500  $\mu$ M ATP or 500  $\mu$ M AMP at 37 °C and analyzed the time course of nucleotide hydrolysis using the malachite green assay. As shown in Fig. 1a, a high level of ecto-phosphohydrolase activity was observed when ATP was used as substrate, but we did not observe the hydrolysis of AMP. We further evaluated the effect of POM-1 on the ecto-ATPase activity of murine macrophages. Cells were pre-incubated for 10 min with 50 or 100  $\mu$ M POM-1 before the addition of substrate, and this concentration was maintained during the reaction. As expected, POM-1 displayed a dose-dependent inhibition of the ecto-ATPase activity in macrophages, with the maximum effect (greater than 70% inhibition) being observed at 100  $\mu$ M after 20 min of reaction (Fig. 1a). We also confirmed the effect of POM-1 on ATP hydrolysis using HPLC. Macrophages were incubated with 3 mM ATP for 30 min in the absence or presence of 100  $\mu$ M POM-1. As can be seen in Fig. 1b, macrophages hydrolyzed 65% of ATP, generating 13% of ADP and 52% of AMP. However, when cells were treated with POM-1, the ATP hydrolysis was only 30%, reducing the production of ADP to 4.5% and AMP to 24%. The absence of AMP hydrolysis in macrophages was also confirmed by HPLC analysis. We used 3 mM AMP as substrate and did not observe any AMPase activity (data not shown).

### POM-1 inhibits free intracellular Ca<sup>2+</sup> increase induced by nucleotides

We used Fura-2 microfluorimetry to investigate the effect of POM-1 on P2Rs of macrophages. In these cells, ATP, ADP, UTP, and UDP induced a rapid and concentration-dependent intracellular Ca<sup>2+</sup> increase, due to Ca<sup>2+</sup> release from intracellular stores (triggered by P2YR activation) or influx from the extracellular medium (dependent of P2XR activation). Under our experimental conditions, ADP elicits a Ca<sup>2+</sup> response in macrophages only at concentrations greater than or equal to 10  $\mu$ M, consistent with the expression of P2Y1R (Fig. 2a). The cells were more responsive to UTP (Fig. 2c) and UDP (Fig. 2e) treatments, with a Ca<sup>2+</sup> response to doses as low as 500 nM, compatible with the activation of P2Y2R, P2Y4R, and P2Y6 [46]. The presence of 100  $\mu$ M POM-1 completely inhibited such responses (Fig. 2b, d, f, respectively).

ATP at concentrations 1–100  $\mu$ M induced a single spike of Ca<sup>2+</sup> after each application (Fig. 3a), a response compatible with the activation of P2Y2R, P2Y4R [46], and P2X1–7Rs [47]. Continuous application of 2 mM ATP at 37 °C induced a sustained increase in the free cytosolic Ca<sup>2+</sup> concentration, a

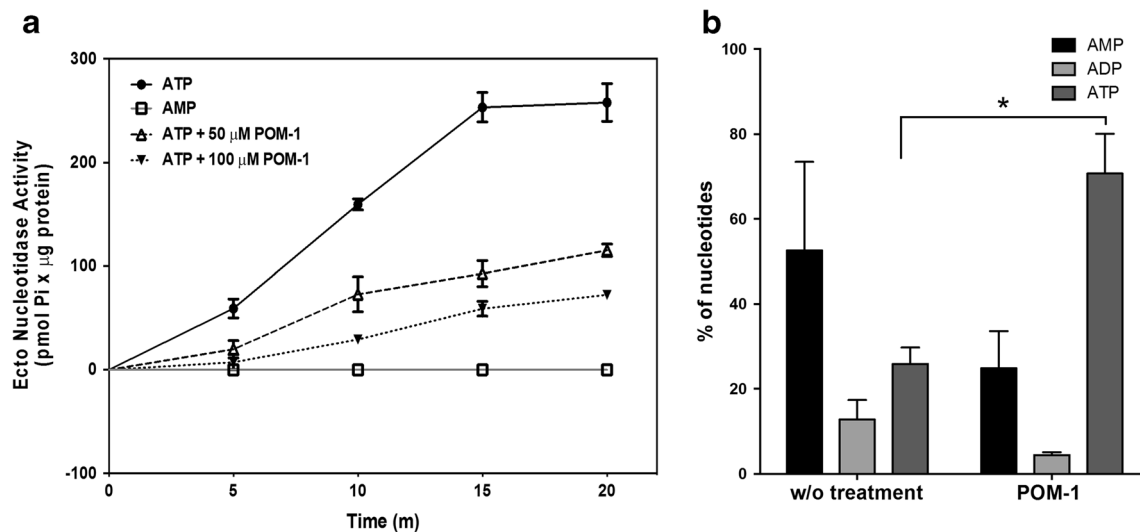


**Fig. 1** Ecto-nucleotidase activity of murine macrophages is inhibited by POM-1. **a** Mouse peritoneal macrophages were incubated for different periods of time at 37 °C in a reaction medium containing the substrates 500 µM AMP (white squares), ATP (dark circles), and also ATP plus 50 µM POM-1 (white triangles, trace lines) or ATP plus 100 µM POM-1 (dark triangles, dotted lines), and the concentration of Pi in the supernatant was analyzed by the malachite green assay. Data are the

means  $\pm$  SD of five independent experiments. **b** Mouse peritoneal macrophages were incubated for 30 min in the presence of 3 mM ATP with or without 100 µM POM-1. The quantity of AMP (black bars), ADP (gray bars), and ATP (dark gray bars) present in the supernatant was analyzed using HPLC. The results are expressed as percentage of control (% initial ATP concentration) and are means  $\pm$  SE of triplicate experiments. \* $p < 0.05$

characteristic of P2X7R activation (Fig. 3c). POM-1 totally inhibited the  $\text{Ca}^{2+}$  response induced by 1 µM ATP and partially inhibited the response induced by 10 and 100 µM ATP (Fig. 3b). No inhibition was observed in the response obtained with 2 mM ATP (Fig. 3d). These results show that POM-1 has a partial inhibitory effect on P2X1–6Rs and suggest that it does not affect the sustained increase of cytosolic  $\text{Ca}^{2+}$  concentration induced by higher doses of ATP and associated with P2X7R activation.

#### POM-1 inhibits the ATP-induced uptake of anionic but not cationic dyes

To further investigate the effects of 100 µM POM-1 on P2X7Rs, we studied P2X7R-induced dye uptake in macrophages using a cationic ([sulforhodamine B (SR-B)]) and an anionic ([carboxyfluorescein (CF)]) dye. In the presence of 5 mM ATP at 37 °C, both dyes could be detected in the cytoplasmic compartment of the cells by fluorescence microscopy and by quantification of the total amount of dye inside the cell using a fluorimetric method (Figs. 4 and 5). The presence of POM-1 had no effect on ATP-induced SR-B uptake (Fig. 4), but this compound showed a significant inhibitory effect on ATP-induced CF uptake, reducing uptake by almost 75% compared with the control (Fig. 5). To confirm these results, we used another cationic dye, EB, and obtained the same results (data not shown). It is important to note that no dye uptake was observed in macrophages obtained from P2X7<sup>-/-</sup> mice, either in the presence or in the absence of POM-1, indicating that this is a

P2X7R-dependent and not a POM-1-induced phenomenon (data not shown). These results support the view that the uptake of anionic and cationic dyes involves different pathways in macrophages and show that POM-1 is only able to inhibit the anionic one.

#### POM-1 inhibits the large ATP-induced channels

P2X7R activation by brief exposure to micromolar concentration of eATP opens a selective cation channel with an 8–9 pS conductance that allows the influx of  $\text{Na}^+$  and  $\text{Ca}^{2+}$  [6]. We performed whole-cell current recordings and observed that 100 µM ATP triggers the typical inward currents (Fig. 6a). When the macrophages were pre-treated with 100 µM POM-1, the same concentration of eATP only induced a smaller current, indicating that POM-1 has partial inhibition of the P2X7R cation channel (Fig. 6b).

We previously identified a P2X7R-associated non-selective channel that is activated by eATP and can be recorded using cell-attached configuration [10]. We therefore investigated whether this large conductance channel could be inhibited by the presence of POM-1. We observed that, whereas the channel opening was detected in the macrophages treated with 5 mM ATP (Fig. 6c), no large conductance channels were observed in the cells treated with the same ATP concentration in the presence of 100 µM POM-1 (Fig. 6d). These results indicate that POM-1 inhibits the large conductance P2X7-associated channel and partially the small conductance cationic channel.

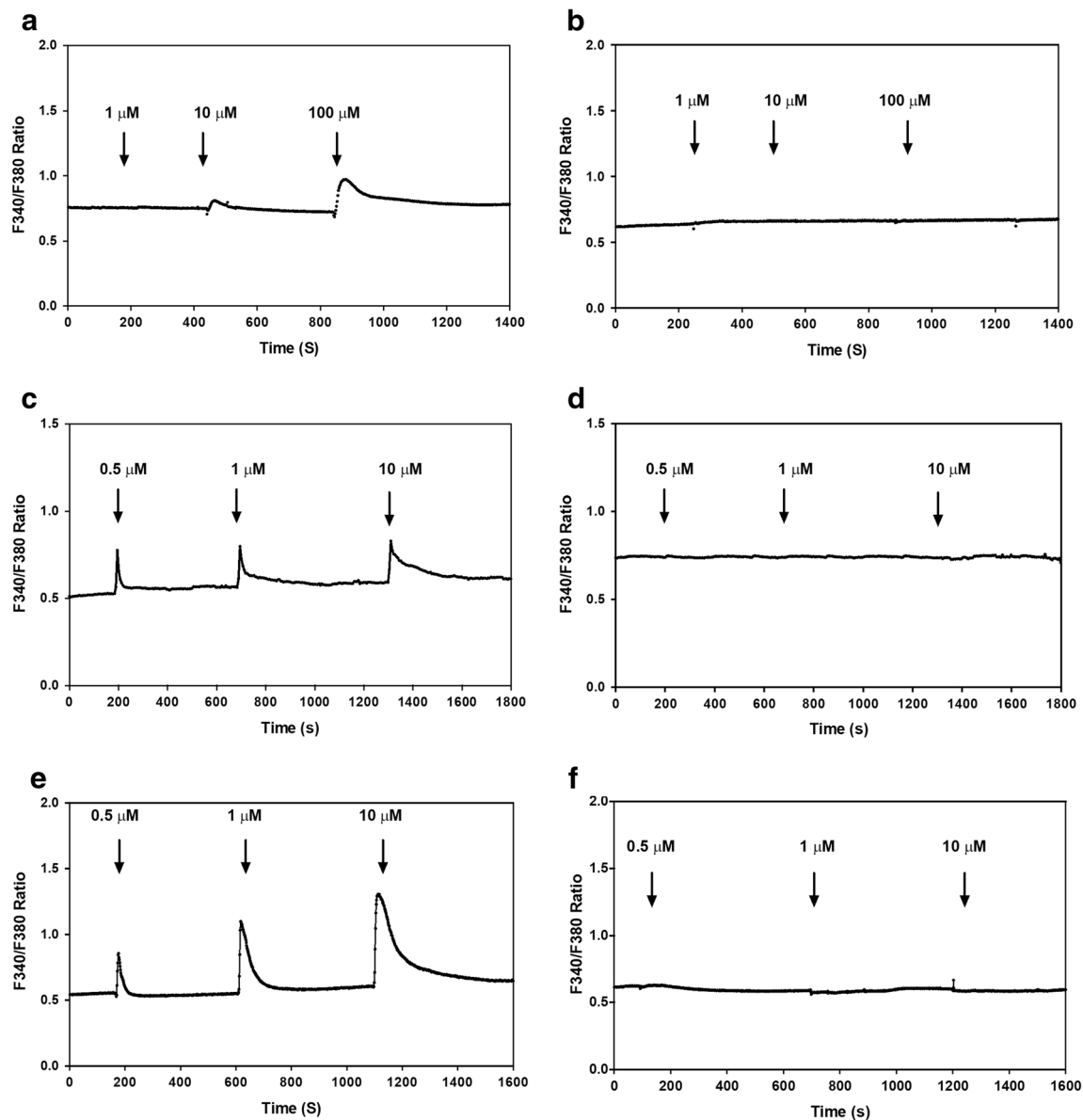


**Fig. 2** Effect of POM-1 on intracellular calcium response induced by ADP, UTP, and UDP in murine macrophages. Mouse peritoneal macrophages were loaded with Fura-2, and 1, 10, and 100  $\mu\text{M}$  ADP (**a, b**); 0.5, 1, and 10  $\mu\text{M}$  UTP (**c, d**); or 0.5, 1, and 10  $\mu\text{M}$  UDP (**e, f**) were added at times indicated with arrows. Cells were pre-incubated and maintained in

the presence of POM-1 (**b, d, f**) and treated with the nucleotides. Fluorescence is proportional to the intracellular calcium concentration and was measured using arbitrary fluorescence ratio units. Representative data of a single experiment are shown. Experiments were repeated at least four times with similar results

### POM-1 inhibits ATP-induced P2X7-associated pyroptosis but not apoptosis

The prolonged activation of P2X7R with millimolar concentrations of eATP triggers cell death, by apoptosis [48] and pyroptosis [49]. Thus, we performed two different experimental protocols that allowed distinguishing between both types of eATP-induced cell death. For apoptotic death induction, macrophages were incubated with 5 mM ATP for 20 min, in the presence or not of 100  $\mu\text{M}$  POM-1 (induction period), washed, and kept in culture medium, without eATP for 6 h more (effector period). Apoptosis was quantified by

measuring the percent of hypodiploid nuclei using flow cytometry, while cell lysis was quantified by LDH release at the end of the effector period. As can be seen in Fig. 7a, the POM-1 treatment did not block the ATP-induced apoptosis.

We evaluated the effects of POM-1 on pyroptosis by treating the macrophages with 100 ng/mL LPS for 6 h, followed by 2 h with 3 mM ATP, in the presence or not of 100  $\mu\text{M}$  POM-1. The measurement of the LDH release showed that POM-1 significantly inhibits the pyroptotic death induced by LPS plus ATP and also the necrotic cell death caused by the incubation with ATP alone for 2 h (Fig. 7b). These results again show a selective inhibition of P2X7R-activated

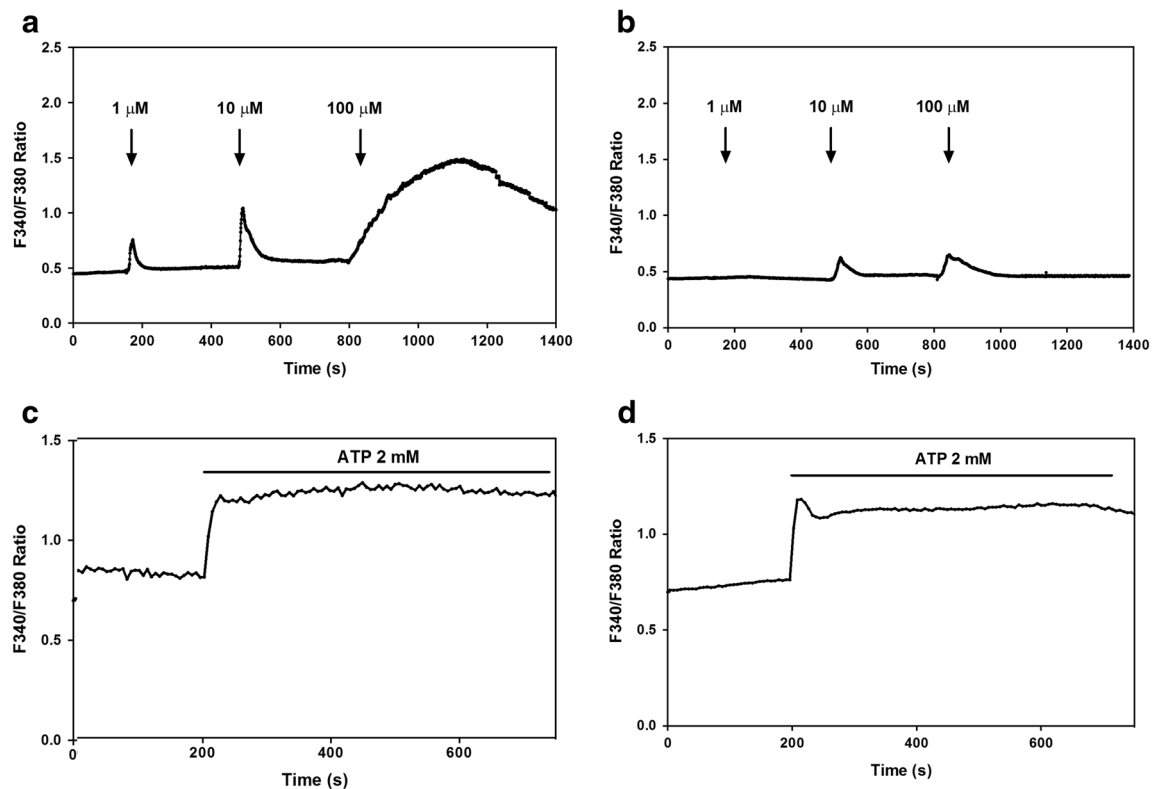


**Fig. 3** Effect of POM-1 on intracellular calcium response induced by ATP in murine macrophages. Mouse peritoneal macrophages were loaded with Fura-2, and 1, 10, and 100  $\mu\text{M}$  ATP (**a**, **b**) were added at the time indicated with arrows. In another set of experiments, cells were maintained at 37  $^{\circ}\text{C}$  and perfused with 2 mM ATP (**c**, **d**), indicated by bars. Some cells were pre-incubated and maintained in the presence of

POM-1 (**b**, **d**) and treated with the nucleotides in the same conditions. Fluorescence is proportional to the intracellular calcium concentration and was measured using arbitrary fluorescence ratio units. Representative data of a single experiment are shown. Experiments were repeated at least four times with similar results

phenomena by POM-1. The treatment only with POM-1 did not cause any difference in macrophage viability.

### Bleb formation in response to ATP is not blocked by POM-1

The activation of P2X7R induces extensive changes in cell morphology, cytoskeletal architecture, and membrane blebbing, a phenomenon defined as the formation of large membrane-bound vesicles, which protrude from the cell surface and are roughly hemispherical and devoid of organelles [50, 51]. To investigate the effect of POM-1 on P2X7R-dependent blebbing phenomena, we treated macrophages with 5 mM ATP in the presence or not of POM-1 and observed the morphological changes after 30 min using DIC microscopy and SEM. Using DIC microscopy, we observed that ATP-treated cells exhibit a substantial change in cell morphology and the formation of membrane blebs (Fig. 8a). The macrophages appeared rounded, with retracted filopodia, and 85% of them showed membrane blebs. In contrast, cells treated with control buffer or POM-1 had numerous filopodia, appeared more elongated, and did not have membrane blebs.

The pre-incubation with POM-1 did not prevent the morphological changes induced by eATP (Fig. 8a, b).

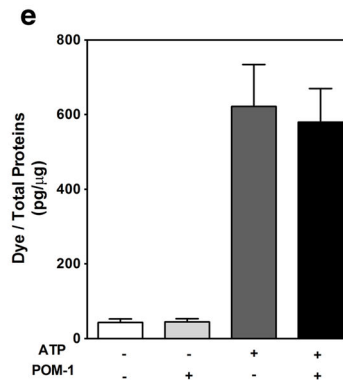
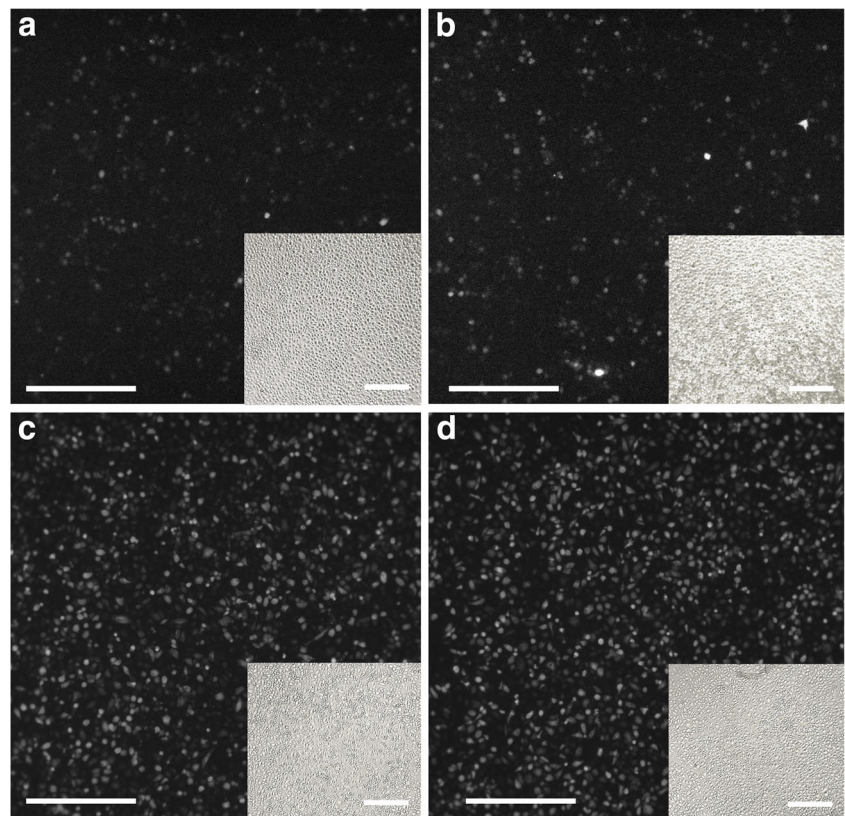
To better characterize the eATP response in macrophages and to observe if there is any morphological change in membrane surface of the cells as a consequence of POM-1 treatment, we performed SEM. As we can see in Fig. 8c, only the macrophages treated with eATP showed bleb formation, even in the presence of POM-1. In the absence of eATP, untreated cells presented similar morphological aspect to that of cells treated with POM-1, showing that POM-1 per se does not cause membrane surface change in macrophages.

### TNF- $\alpha$ , IL-1 $\beta$ , and NO release in LPS-primed macrophages is blocked by POM-1

eATP, acting via P2X7R, induces production and release of IL-1 $\beta$  by activation of the NLRP3/caspase-1 complex [13]. We examined the effects of POM-1 on IL-1 $\beta$  and TNF- $\alpha$  secretion by LPS-primed macrophages in response to 3 mM ATP. Macrophages treated with 100  $\mu\text{M}$  POM-1 displayed a significant decrease in ATP-induced IL-1 $\beta$  release compared to cells without treatment (Fig. 9a). In our conditions, LPS with or without eATP can lead to TNF- $\alpha$  release, which was



**Fig. 4** eATP-induced sulforhodamine B uptake in murine macrophages is inhibited by POM-1. Fluorescence microscopy of mouse peritoneal macrophages incubated for 15 min at 37 °C in the absence (a, b) or in the presence (c, d) of 5 mM ATP, with (b, d) or without (a, c) 100  $\mu$ M POM-1. In all cases, SR-B (200  $\mu$ M) was added and the samples were washed before transfer to the microscope stage. **e** Quantitative comparison of uptake of SR-B in the presence or not of POM-1. Cells were incubated at 37 °C with SR-B for 10 min in the presence of 5 mM ATP, with or without POM-1, as indicated, and the amount of dye taken up by the cells was measured by spectrofluorimetry, as described in the “Material and methods” section. The bars represent the means of four independent experiments. Scale bars = 200  $\mu$ m



also observed by others [52]. Both types of stimulation were inhibited by pre-treatment with POM-1, blocking TNF- $\alpha$  production by macrophages (Fig. 9b).

We next tested whether POM-1 inhibits LPS-induced production of NO, a process that may involve the release of ATP and the activation of P2 receptors [53, 54]. For that, macrophages were incubated for 24 h with different concentration of LPS in the absence or presence of 100  $\mu$ M POM-1, and the release of NO was quantified indirectly by measuring nitrite, the product of the reaction of NO with oxygen. POM-1 inhibited the release of NO at all the concentrations of LPS tested (Fig. 9c).

Taken together, these results indicate that POM-1 has a potent anti-inflammatory effect on macrophages.

## Discussion

NTPDase1 (CD39) is the dominant ecto-nucleotidase expressed in murine peritoneal macrophages elicited with thioglycollate, as shown by Lévesque and collaborators using RT-PCR and western blot, and who did not detect the presence of CD73 in this cell type [55]. Zanin and co-workers showed that CD73 is expressed in resident, LPS-stimulated and IL-4-stimulated macrophages, but did not detect any AMPase activity or expression in thioglycollate-elicited macrophages [56]. Consistent with these previous data, we found that thioglycollate-elicited murine macrophages have ecto-ATPase activity compatible with CD39, but we did not detect AMP hydrolysis, consistent with the lack of at CD73 activity

**Fig. 5** POM-1 does not affect eATP-induced carboxyfluorescein uptake in murine macrophages. Fluorescence microscopy of mouse peritoneal macrophages incubated for 15 min at 37 °C in the absence (a, b) or in the presence (c, d) of 5 mM ATP, with (b, d) or without (a, c) 100  $\mu$ M POM-1. In all cases, CF (5 mM) was added and the samples were washed before transfer to the microscope stage. **e** Quantitative comparison of uptake of CF in the presence or not of POM-1. Cells were incubated at 37 °C with CF for 10 min in the presence of 5 mM ATP, with or without POM-1, as indicated, and the amount of dye taken up by the cells was measured by spectrofluorimetry as described in the “Material and methods” section. The bars represent the means of four independent experiments. Scale bars = 200  $\mu$ m

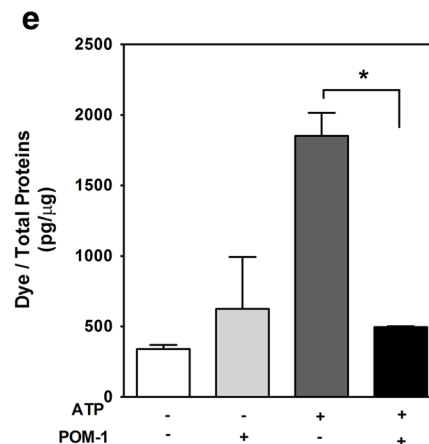
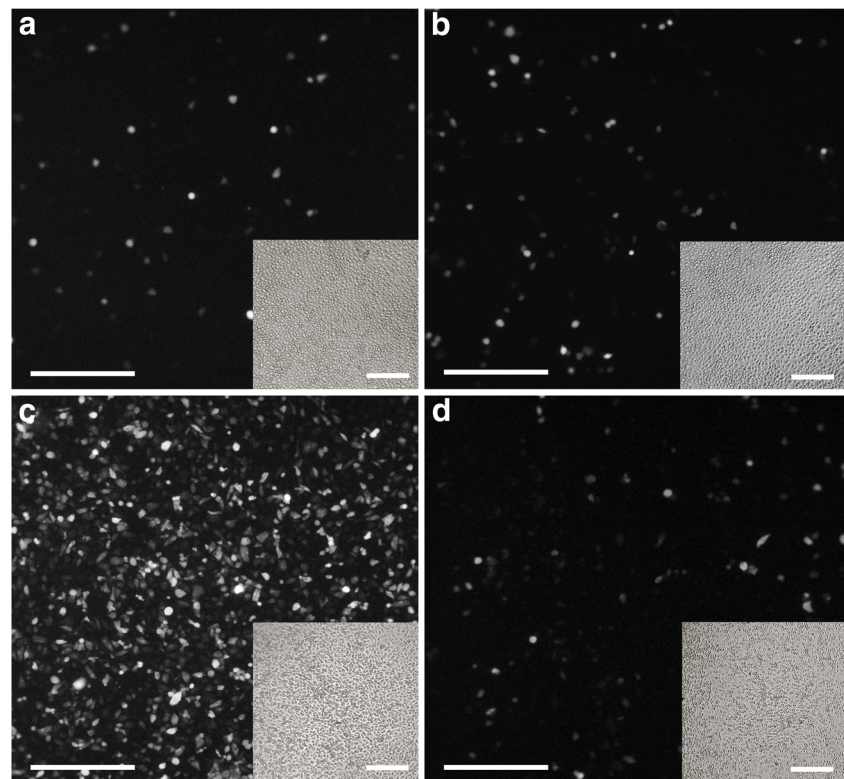


(Fig. 1). Moreover, the ATP hydrolysis was inhibited by 100  $\mu$ M POM-1, as expected [57].

The CD39 activity has potent implications for inflammation, due to the reduction of the eATP levels. So, POM-1, as a CD39 inhibitor, is expected to increase the inflammatory response of macrophages. However, our data show that POM-1 has anti-inflammatory effects on these cells. This suggests that the effects of POM-1 on macrophage inflammatory response could be due to the inhibition of P2 receptors.

Extracellular ATP, ADP, UDP, and UTP can induce cytosolic  $\text{Ca}^{2+}$  elevation in macrophages through the activation of  $G_q$ -coupled P2Y and P2X receptors [58]. In our conditions, extracellular application of ATP, ADP, UTP, and UDP induced elevations of free intracellular  $\text{Ca}^{2+}$  concentrations at doses

consistent with the activation of P2Y1, 2, 4, and 6, in agreement with previously published results [59]. POM-1 inhibited the cytosolic  $\text{Ca}^{2+}$  elevation induced by all these P2Y receptors (Fig. 2). eATP can also induce the influx of extracellular  $\text{Ca}^{2+}$  through P2X1–7 channels, most of them previously described in peritoneal macrophages [59]. Here, we showed that POM-1 can partially inhibit the spike of  $\text{Ca}^{2+}$  response triggered by P2X1–6, but not the sustained  $\text{Ca}^{2+}$  increase evoked by the P2X7R activation (Fig. 3).

We previously described that P2X7R activation in macrophages is associated with two different transport mechanisms through the plasma membrane: a diffusional pathway, which allows the entry of anions, and another pathway for non-diffusional uptake of cations [10]. In HEK-

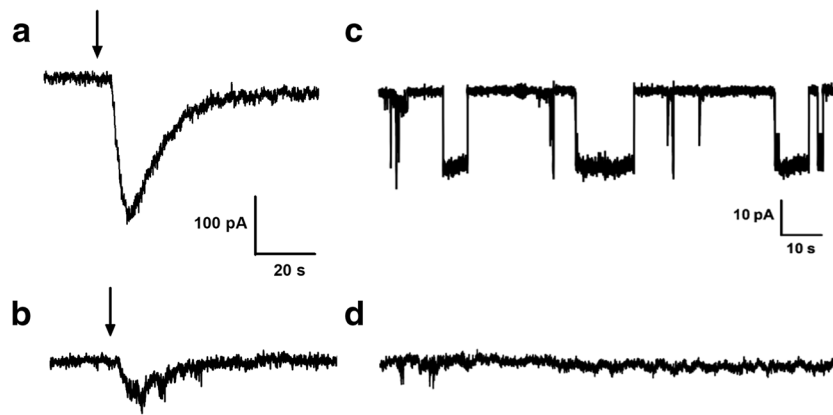


**Fig. 6** Effect of POM-1 on eATP-induced ionic currents. Currents evoked by 100  $\mu\text{M}$  ATP in murine macrophages, under voltage clamp at  $-40$  mV, using whole-cell mode, in the absence (a) or presence of 100  $\mu\text{M}$  POM-1 (b). Single-channel currents activated by 4 mM ATP,

under voltage clamp at  $-40$  mV, using cell-attached mode, in the absence (c) or presence of 100  $\mu\text{M}$  POM-1 (d). Representative data of a single experiment are shown. Experiments were repeated at least four times with similar results

293 cells transfected with P2X7R, we observed the uptake of cationic dyes and sustained increase in cytosolic  $\text{Ca}^{2+}$  levels, as well as the ionic inward currents typically associated with the activation of this receptor. In the same previous study, we showed that P2X7R-transfected HEK cells do not present uptake of anionic dyes or opening of large conductance P2X7R-associated channel [10]. In the present study, POM-1 inhibited the uptake of anionic fluorescent dyes (Fig. 5) and the activity of the large conductance ATP-dependent channels (Fig. 6), but not cationic dye uptake or changes in intracellular  $\text{Ca}^{2+}$  concentration in

thioglycollate-elicited murine macrophages stimulated with 2 mM ATP (Figs. 3 and 4). These results add additional support to the existence of these two distinct P2X7R-dependent pathways for molecule uptake and suggest that POM-1 is a new pharmacological tool to study them. We previously also showed that ATP-induced cationic dye uptake in macrophages does not require intracellular  $\text{Ca}^{2+}$  signals [60]. However, the link between the cytosolic  $\text{Ca}^{2+}$  elevations, the solute transport mechanisms induced by extracellular nucleotides, and the cellular responses evoked by them in macrophages is not yet clear.

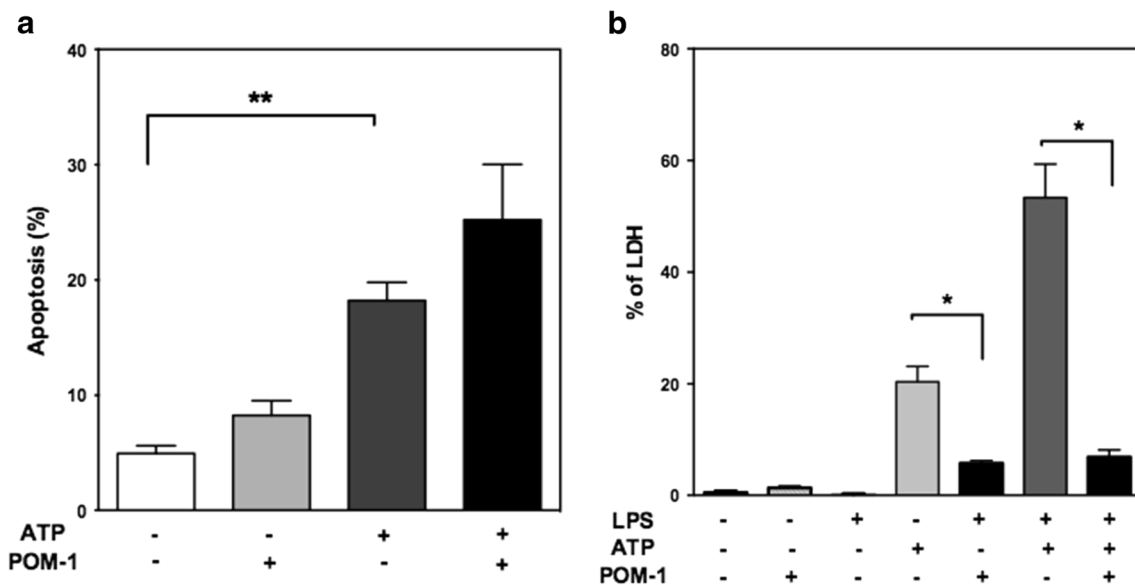


**Fig. 7** eATP-induced cell death in the presence or not of POM-1. Murine macrophages were exposed to zero or 5 mM ATP, with or without addition of 100  $\mu\text{M}$  POM-1 for 20 min, washed, and maintained in culture for 6 h. After that, macrophages were incubated with apoptosis buffer containing EB and the nuclei were analyzed by flow cytometry. The percentage of apoptosis was calculated according to the number of hypodiploid events, considering the result obtained with 5 mM ATP as 100% (a). Cells were pre-incubated or not with 100  $\mu\text{M}$  POM-1 for

30 min and treated with 100 ng/mL LPS for 6 h and with 3 mM ATP for 2 h. Macrophages were also treated only with POM-1 for 8 h, ATP for 2 h, or LPS for 6 h. LDH activity was measured in the supernatants. Control lyses were obtained by using supernatants of untreated cells (0%), and cells treated with 1% saponin for 30 min (100%) (b). Data are the means  $\pm$  SE of at least four independent experiments. \* $p < 0.01$ ; \*\* $p < 0.0001$

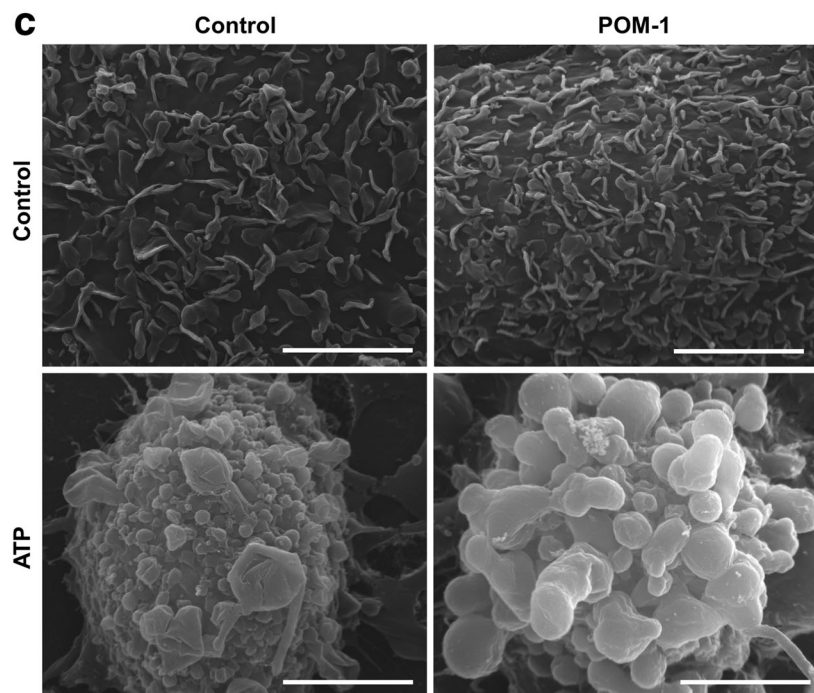
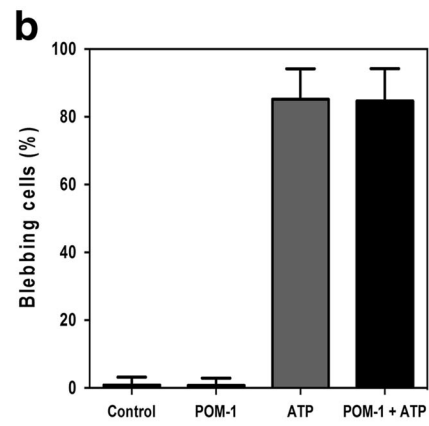
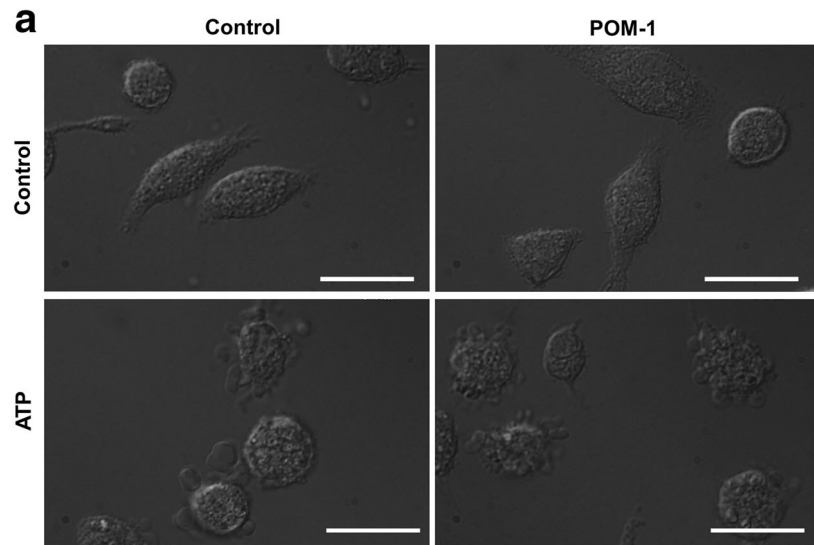




**Fig. 8** POM-1 does not affect membrane blebbing induced by eATP in macrophages. Murine macrophages were plated on glass coverslips and treated with saline solution (control) or 5 mM ATP for 30 min, with or without 100  $\mu$ M POM-1, washed, and visualized using light microscopy or processed for SEM. **a** Images obtained using differential interference contrast (DIC). Scale bars 7  $\mu$ m. **b** Cells from five random fields were counted and scored for blebbing. The graph represents the mean percentages of macrophages that were positive for blebbing + ES, from four independent experiments. **c** Scanning electron microscopy of macrophages with the different treatments. Scale bars 5  $\mu$ m

Priming of macrophages with LPS induces intracellular accumulation of pro-IL-1 $\beta$  and pro-IL-18, which will be released after eATP stimulation. P2X7R activation promotes assembly of inflammasome, caspase-1-dependent cleavage,

and release of biologically active cytokines [61]. In addition, caspase-1 activation induces pyroptotic cell death [62] and activates NF- $\kappa$ B [63], leading to the secretion of TNF- $\alpha$  [64] and NO production [65]. It is important to mention that caspase-1 induces NF- $\kappa$ B activation independently of its enzymatic role in cytokine maturation [63]. Our results show that POM-1 inhibits the sequence of events triggered by eATP via P2X7R activation in LPS-primed macrophages, since this drug can prevent LDH (Fig. 7b), IL-1 $\beta$ , TNF- $\alpha$ , and NO release (Fig. 9). Interestingly, POM-1 is also able to inhibit the release of TNF- $\alpha$  and NO even without eATP treatment, suggesting that this compound can block the canonical LPS-induced NF- $\kappa$ B activation mediated by TLR4-MyD88 signaling pathway. However, in these conditions, one must also

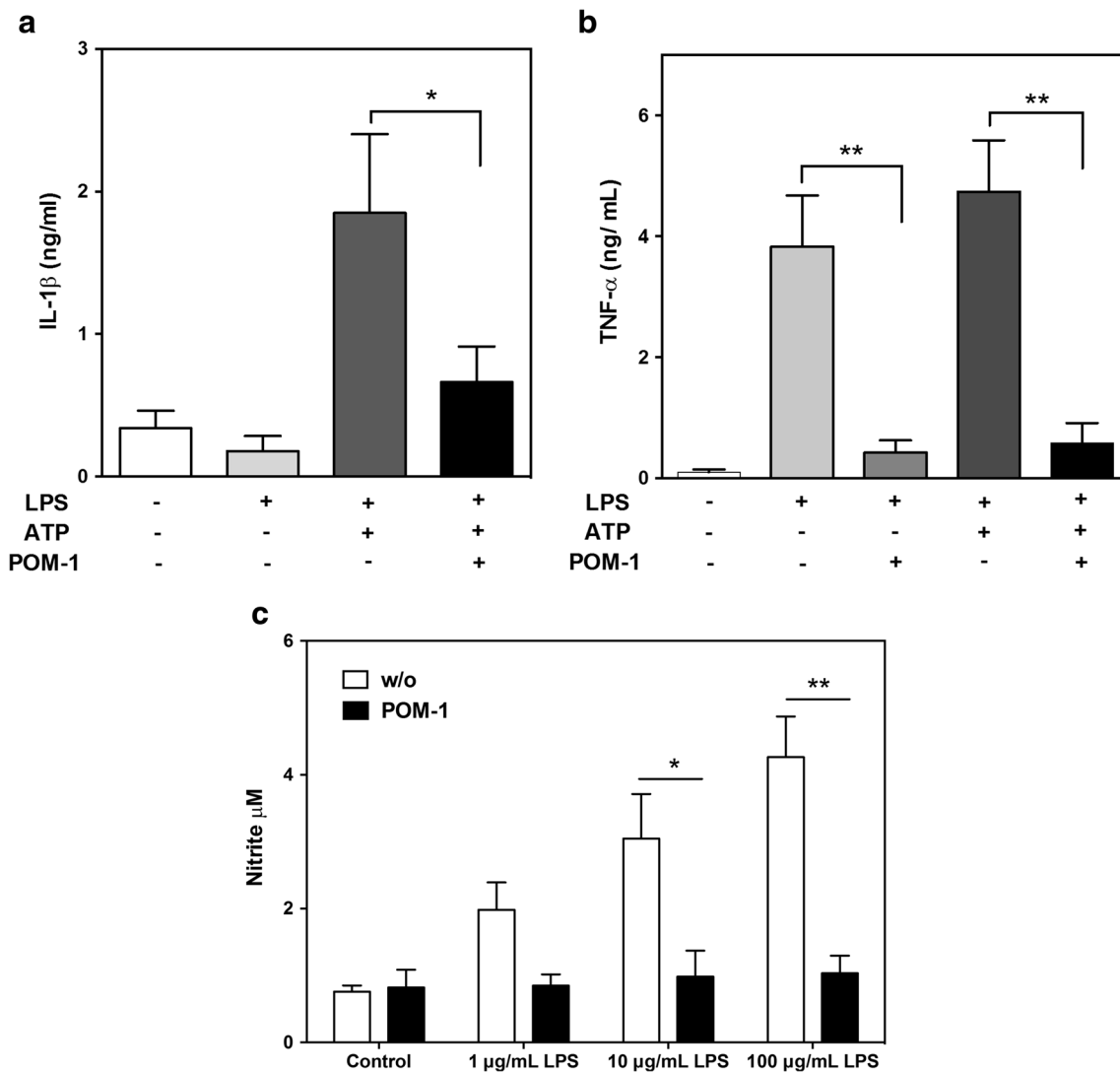


**Fig. 9** POM-1 blocks TNF- $\alpha$ , IL-1 $\beta$ , and NO release in LPS-primed macrophage. Peritoneal mouse macrophages were incubated with LPS (100 ng/mL) for 6 h, finally adding ATP (3 mM) for 2 h. In the cases indicated, 100  $\mu$ M POM-1 was present in the culture medium all the time. The supernatants were collected, and the cytokine measured by an ELISA detection kit for IL-1 $\beta$  (a) or TNF- $\alpha$  (b). For the NO measurements,

macrophages were treated with LPS (at the indicated concentrations) for 24 h, in the presence or not of 100  $\mu$ M POM-1. The supernatant was collected, and the NO released was measured by the Griess method. Data are the means  $\pm$  SE of five independent experiments. \* $p$  < 0.01; \*\* $p$  < 0.001



consider the possibility that the LPS stimulation triggers ATP release by the macrophages, as previously shown [53, 54].

Peritoneal macrophages from *Entpd1*<sup>-/-</sup> mice are more susceptible to ATP-induced necrotic cell death and release more IL-1 $\beta$  when stimulated with LPS plus ATP, compared with macrophages from wild-type mice [55]. This finding indicates that the effect of POM-1 in decreasing P2X7-dependent cell death and cytokine release is not caused by inhibition of CD39 activity.

On the other hand, stimulation of P2X7R also activates the caspase-8/9/3 pathway and triggers apoptotic cell death [66]. Hanley and collaborators showed that activation of P2X7R induces blebbing, uptake of cationic dyes, caspase-3/7 activation, and cell death independent of caspase-1 and pannexin-1 [67]. P2X7R-dependent blebbing involves both Ca<sup>2+</sup>-dependent and Ca<sup>2+</sup>-independent mechanisms [52, 68–70] and is dissociated from IL-1 $\beta$  secretion or caspase-1 activation [52]. In accordance with that second pathway activated by P2X7R, we did not observe POM-1 inhibition of cationic uptake (Fig. 4a), apoptosis (Fig. 7a), or bleb formation (Fig. 8) in

macrophages treated with ATP. Also, our results are in concordance with previous data, which showed the existence of two different pathways for P2X7R-induced cell death, with separate intracellular signaling events for apoptosis and LDH release [49]. Based on the results obtained so far, a hypothetical model for P2X7R intracellular pathway and POM-1 inhibition is presented in Fig. 10.

The role of pannexin-1 in the signaling cascades that mediate the different responses to P2X7R activation in macrophages remains unknown. One difficulty in the effort to better understand this question is the fact that often researchers use the ATP-dependent cationic dye uptake as a measure of pannexin-1 involvement in a particular phenomenon [9, 67, 71]. However, we [10] and others [11] showed that the P2X7-dependent dye uptake has at least two associated pathways, with differences between cations and anions. The participation of pannexin-1 in each transport mechanism stays unclear.

The activation of pannexin-1 channels has been associated with activation of NLRP3 inflammasome/caspase-1 and the induction of cell death and cytokine release [9, 71]. However,

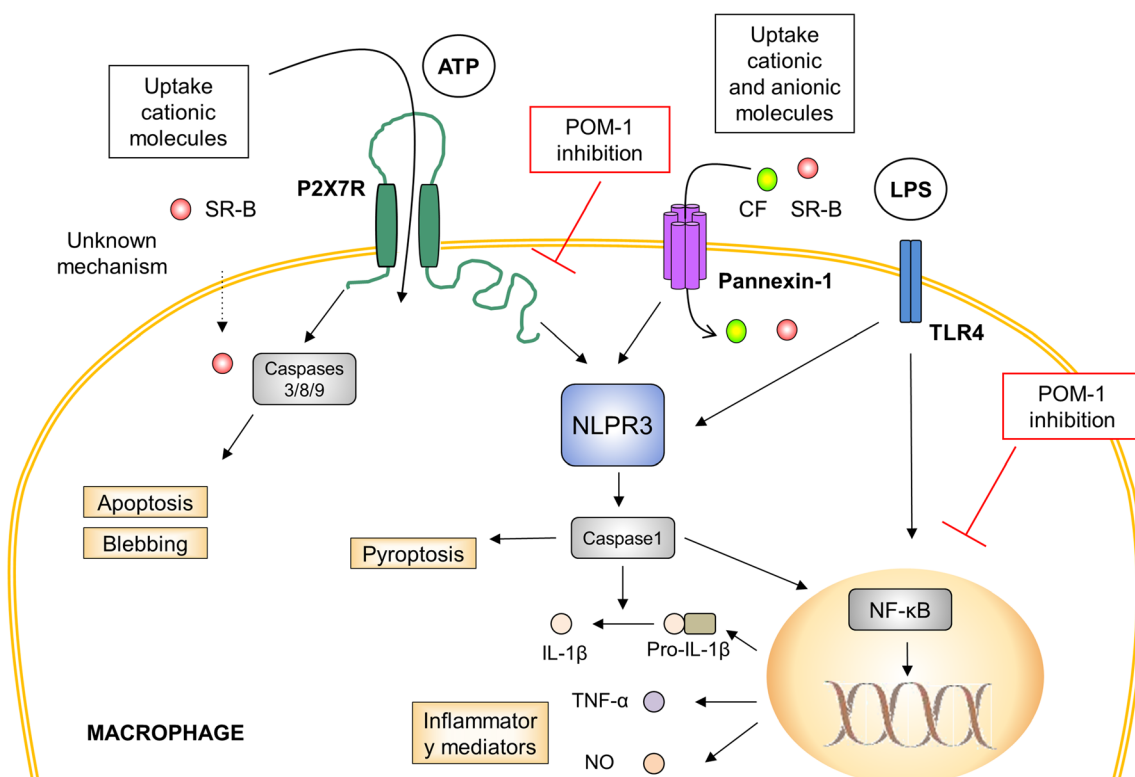


**Fig. 10** Hypothetic model for of POM-1 inhibition of P2X7R intracellular pathways. P2X7R activation by eATP leads to the entry of extracellular Na<sup>+</sup> and Ca<sup>2+</sup>. Prolonged exposure to millimolar concentrations of eATP triggers the opening of different transport mechanisms, which allow the passage of larger molecules, such as the anionic carboxifluorescein (CF) and the cationic sulforhodamine-B (SR-B) dye. Different intracellular cascades are also triggered. We propose two major separated pathways dependent on P2X7R. One sequence of events includes the activation of caspase-3, caspase-8, and caspase-9, resulting in the induction of membrane blebbing and apoptosis. This

cascade is associated with uptake of large cationic molecules and cannot be inhibited by POM-1. The other intracellular pathway triggered by P2X7R involves the inflammasome assembly, with caspase-1 activation and induction of release of cytokines (TNF- $\alpha$ , IL-1 $\beta$ ), nitric oxide (NO), and pyroptosis. This cascade is associated with the uptake of both large cationic and anionic molecules and can be inhibited by POM-1. Because the TNF- $\alpha$  and NO release triggered by LPS are also inhibited by POM-1, an effect of this compound on the TLR4 canonical pathway should be considered

Qu and colleagues showed that the activation of caspase-1 and secretion of IL-1 $\beta$  in response to ATP are normal in pannexin-1-deficient macrophages [72].

Non-canonical inflammasome activates another class of inflammatory caspases, including caspase-11, to induce pyroptosis and promote IL-1 $\beta$  by triggering the canonical NLRP3 inflammasome [73]. Recently, Yang and collaborators presented data indicating that pannexin-1 and P2X7R are required for susceptibility to endotoxic shock in mice induced via the non-canonical inflammasome pathway [74]. However, how P2X7R regulates the caspase-11 activation and what the role of pannexin-1 in this process is not known yet.

POM-1 can inhibit the events related with ATP-dependent inflammasome activation, anionic dye uptake, and also the opening of large conductance channels, which are associated with P2X7R-dependent pannexin-1 activation. Considering that, it seems reasonable to think that these phenomena occur in the same signaling pathway dependent on P2X7R, different from the pathway that includes triggering of apoptosis, blebbing, and cationic dye uptake, which cannot be inhibited by POM-1 (Fig. 10).

**Acknowledgements** We thank the National Institute of Science and Technology for Structural Biology and Bioimaging—Microscopy Division (CENABIO-UFRJ) for allowing use of the scanning electron microscope.

**Funding information** This research received financial support from CNPq, FAPERJ and FINEP.

#### Compliance with ethical standards

**Conflicts of interest** Gabriela Pimenta-dos-Reis declares that she has no conflict of interest.

Eduardo José Lopes Torres declares that he has no conflict of interest.

Paula Gabriela Quintana declares that she has no conflict of interest.

Lincon Onorio Vidal declares that he has no conflict of interest.

Bárbara Andréa Fortes dos Santos declares that she has no conflict of interest.

Chuan-Sheng Lin declares that he has no conflict of interest.

Norton Heise declares that he has no conflict of interest.

Pedro Muanis Persechini declares that he has no conflict of interest.

Julietta Schachter declares that she has no conflict of interest.

**Ethical approval** All animals were used according to the guidelines for animal use in scientific experiments of the Carlos Chagas Filho Institute of Biophysics of Federal University of Rio de Janeiro. The protocols were approved by the Research Ethics Committee on Animal Care of the Health Science Center of Federal University of Rio de Janeiro (protocol number 001200.001568/2013-87).

## References

1. Junger WG (2011) Immune cell regulation by autocrine purinergic signaling. *Nat Rev Immunol* 11:201–212. <https://doi.org/10.1038/nri2938>
2. Burnstock G, Boeynaems JM (2014) Purinergic signalling and immune cells. *Purinergic Signal* 10:529–564. <https://doi.org/10.1007/s11302-014-9427-2>
3. Burnstock G (2014) Purinergic signalling: from discovery to current developments. *Exp Physiol* 99:16–34. <https://doi.org/10.1113/expphysiol.2013.071951>
4. Khakh BS, North RA (2006) P2X receptors as cell-surface ATP sensors in health and disease. *Nature* 442:527–532. <https://doi.org/10.1038/nature04886>
5. Di Virgilio F, Vuerich M (2015) Purinergic signaling in the immune system. *Auton Neurosci* 191:117–123. <https://doi.org/10.1016/j.autneu.2015.04.011>
6. North RA (2002) Molecular physiology of P2X receptors. *Physiol Rev* 82:1013–1067. <https://doi.org/10.1152/physrev.00015.2002>
7. Virginio C, MacKenzie A, North RA, Surprenant A (1999) Kinetics of cell lysis, dye uptake and permeability changes in cells expressing the rat P2X7 receptor. *J Physiol Lond* 519:335–346. <https://doi.org/10.1111/j.1469-7793.1999.0335m.x>
8. Coutinho-Silva R, Persechini PM (1997) P2Z purinoceptor-associated pores induced by extracellular ATP in macrophages and J774 cells. *Am J Phys* 273:C1793–C1800
9. Pelegrin P, Surprenant A (2006) Pannexin-1 mediates large pore formation and interleukin-1 $\beta$  release by the ATP-gated P2X7 receptor. *EMBO J* 25:5071–5082. <https://doi.org/10.1038/sj.emboj.7601378>
10. Schachter J, Motta AP, de Souza Zamorano A, da Silva-Souza HA, Guimarães MZ, Persechini PM (2008) ATP-induced P2X7-associated uptake of large molecules involves distinct mechanisms for cations and anions in macrophages. *J Cell Sci* 121:3261–3270. <https://doi.org/10.1242/jcs.029991>
11. Cankurtaran-Sayar S, Sayar K, Ugur M (2009) P2X7 receptor activates multiple selective dye-permeation pathways in RAW 264.7 and human embryonic kidney 293 cells. *Molecular Pharmacol* 76:1323–1332. <https://doi.org/10.1124/mol.109.059923>
12. Li M, Toombes GE, Silberberg SD, Swartz KJ (2015) Physical basis of apparent pore dilation of ATP-activated P2X receptor channels. *Nat Neurosci* 18:1577–1583. <https://doi.org/10.1038/nn.4120>
13. Csóka B, Németh ZH, Törö G, Idzko M, Zech A, Koscsó B, Spolarics Z, Antonioli L, Cseri K, Erdélyi K, Pacher P, Haskó G (2015) Extracellular ATP protects against sepsis through macrophage P2X7 purinergic receptors by enhancing intracellular bacterial killing. *FASEB J* 29:3626–3637. <https://doi.org/10.1096/fj.15-272450>
14. Di Virgilio F, Chiozzi P, Ferrari D, Falzoni S, Sanz JM, Morelli A, Torboli M, Bolognesi G, Baricordi OR (2001) Nucleotide receptors: an emerging family of regulatory molecules in blood cells. *Blood* 97:587–600. <https://doi.org/10.1182/blood.V97.3.587>
15. Coutinho-Silva R, Stahl L, Raymond MN, Jungas T, Verbeke P, Burnstock G, Darville T, Ojcius DM (2003) Inhibition of chlamydial infectious activity due to P2X7R-dependent phospholipase D activation. *Immunity* 19:403–412. [https://doi.org/10.1016/S1074-7613\(03\)00235-8](https://doi.org/10.1016/S1074-7613(03)00235-8)
16. Ferrari D, Pizzirani C, Adinolfi E, Lemoli RM, Curti A, Idzko M, Panther E, Di Virgilio F (2006) The P2X7 receptor: a key player in IL-1 processing and release. *J Immunol* 176:3877–3883. <https://doi.org/10.4049/jimmunol.176.7.3877>
17. Pfeiffer ZA, Aga M, Prabhu U, Watters JJ, Hall DJ, Bertics PJ (2004) The nucleotide receptor P2X7 mediates actin reorganization and membrane blebbing in RAW 264.7 macrophages via p38 MAP kinase and Rho. *J Leukoc Biol* 75:1173–1182. <https://doi.org/10.1189/jlb.1203648>
18. Zimmermann H, Zebisch M, Sträter N (2012) Cellular function and molecular structure of ecto-nucleotidases. *Purinergic Signal* 5:437–502. <https://doi.org/10.1007/s11302-012-9309-4>

19. Dwyer KM, Deaglio S, Gao W, Friedman D, Strom TB, Robson SC (2007) CD39 and control of cellular immune responses. *Purinergic Signal* 3:171–180. <https://doi.org/10.1007/s11302-006-9050-y>
20. Morandini AC, Savio LE, Coutinho-Silva R (2014) The role of P2X7 receptor in infectious inflammatory diseases and the influence of ectonucleotidases. *Biom J* 37:169–177. <https://doi.org/10.4103/2319-4170.127803>
21. Antonioli L, Yegutkin GG, Pacher P, Blandizzi C, Hasko G (2016) Anti-CD73 in cancer immunotherapy: awakening new opportunities. *Trends Cancer* 2:95–109. <https://doi.org/10.1016/j.trecan.2016.01.003>
22. Schachter J, Delgado KV, Barreto-de-Souza V, Bou-Habib DC, Persechini PM, Meyer-Fernandes JR (2015) Inhibition of ecto-ATPase activities impairs HIV-1 infection of macrophages. *Immunobiology* 220(5):589–596. <https://doi.org/10.1016/j.imbio.2014.12.004>
23. Baqi Y (2015) Ecto-nucleotidase inhibitors: recent developments in drug discovery. *Mini Rev Med Chem* 15:21–33. <https://doi.org/10.2174/1389557515666150219115141>
24. Munkonda MN, Kauffenstein G, Kukulski F, Lévesque SA, Legendre C, Pelletier J, Lavoie EG, Lecka J, Sévigny J (2007) Inhibition of human and mouse plasma membrane bound NTPDases by P2 receptor antagonists. *Biochem Pharmacol* 74: 1524–1534. <https://doi.org/10.1016/j.bcp.2007.07.033>
25. Dunn PM, Blakeley AG (1988) Suramin: a reversible P2-purinoreceptor antagonist in the mouse vas deferens. *Br J Pharmacol* 93:243–245
26. Chen BC, Lee CM, Lin WW (1996) Inhibition of ecto-ATPase by PPADS, suramin and reactive blue in endothelial cells, C6 glioma cells and RAW 264.7 macrophages. *Br J Pharmacol* 119:1628–1634
27. Gendron FP, Benrezzak O, Krugh BW, Kong Q, Weisman GA, Beaudoin AR (2002) Purine signaling and potential new therapeutic approach: possible outcomes of NTPDase inhibition. *Curr Drug Targets* 3:229–245. <https://doi.org/10.2174/1389450023347713>
28. Lee SY, Fiene A, Li W, Hanck T, Brylev KA, Fedorov VE, Lecka J, Haider A, Pietzsch HJ, Zimmermann H, Sévigny J, Kortz U, Stephan H, Müller CE (2015) Polyoxometalates-potent and selective ecto-nucleotidase inhibitors. *Biochem Pharmacol* 15:171–181. <https://doi.org/10.1016/j.bcp.2014.11.002>
29. Kohler D, Eckle T, Faigle M, Grenz A, Mittelbronn M, Laucher S, Hart ML, Robson SC, Müller CE, Eltzschig HK (2007) CD39/ectonucleoside triphosphate diphosphohydrolase 1 provides myocardial protection during cardiac ischemia/reperfusion injury. *Circulation* 116:1784–1794. <https://doi.org/10.1161/CIRCULATIONAHA.107.690180>
30. Grenz A, Zhang H, Hermes M, Eckle T, Klingel K, Huang DY, Müller CE, Robson SC, Osswald H, Eltzschig HK (2007) Contribution of E-NTPDase1 (CD39) to renal protection from ischemia-reperfusion injury. *FASEB J* 21:2863–2873. <https://doi.org/10.1096/fj.06.7947com>
31. Müller CE, Iqbal J, Baqi Y, Zimmermann H, Röllich A, Stephan H (2006) Polyoxometalates—a new class of potent ecto-nucleoside triphosphate diphosphohydrolase (NTPDase) inhibitors. *Bioorg Med Chem Lett* 16:5943–5947. <https://doi.org/10.1016/j.bmcl.2006.09.003>
32. Zhai F, Li D, Zhang C, Wang X, Li R (2008) Synthesis and characterization of polyoxometalates loaded starch nanocomplex and its antitumoral activity. *Eur J Med Chem* 43:1911–1917. <https://doi.org/10.1016/j.ejmech.2007.11.032>
33. Seko A, Yamase T, Yamashita K (2009) Polyoxometalates as effective inhibitors for sialyl- and sulfotransferases. *J Inorg Biochem* 103:1061–1066. <https://doi.org/10.1016/j.jinorgbio.2009.05.002>
34. Turner TL, Nguyen VH, McLaughlan CC, Dymon Z, Dorsey BM, Hooker JD, Jones MA (2012) Inhibitory effects of decavanadate on several enzymes and *Leishmania tarentolae* in vitro. *J Inorg Biochem* 108:96–104. <https://doi.org/10.1016/j.jinorgbio.2011.09.009>
35. Qi Y, Xiang Y, Wang J, Qi Y, Li J, Niu J, Zhong J (2013) Inhibition of hepatitis C virus infection by polyoxometalates. *Antivir Res* 100: 392–398. <https://doi.org/10.1016/j.antiviral.2013.08.025>
36. Nomiya K, Torii H, Hasegawa T, Nemoto Y, Nomura K, Hashino K, Uchida M, Kato Y, Shimizu K, Oda M (2001) Insulin mimetic effect of a tungstate cluster. Effect of oral administration of homopolyoxotungstates and vanadium-substituted polyoxotungstates on blood glucose level of STZ mice. *J Inorg Biochem* 86:657–667. [https://doi.org/10.1016/S0162-0134\(01\)00233-1](https://doi.org/10.1016/S0162-0134(01)00233-1)
37. Amobi NI, Guillebaud J, Smith IC (2012) Perspective on the role of P2X-purinoreceptor activation in human vas deferens contractility. *Exp Physiol* 97:583–602. <https://doi.org/10.1113/expphysiol.2011.063206>
38. Pinheiro AR, Paramos-de-Carvalho D, Certal M, Costa C, Magalhães-Cardoso MT, Ferreira F, Costa MA, Correia-de-Sá P (2013) Bradykinin-induced Ca<sup>2+</sup> signaling in human subcutaneous fibroblasts involves ATP release via hemichannels leading to P2Y12 receptors activation. *Cell Commun Signal* 18:70. <https://doi.org/10.1186/1478-811X-11-70>
39. Wan P, Liu X, Xiong Y, Ren Y, Chen J, Lu N, Guo Y, Bai A (2016) Extracellular ATP mediates inflammatory responses in colitis via P2X7 receptor signaling. *Sci Rep* 6:19108. <https://doi.org/10.1038/srep19108>
40. Lanzetta PA, Alvarez LJ, Reinach PS, Candia OA (1979) An improved assay for nanomole amounts of inorganic phosphate. *Anal Biochem* 100:95–97. [https://doi.org/10.1016/0003-2697\(79\)90115-5](https://doi.org/10.1016/0003-2697(79)90115-5)
41. Russo-Abrahão T, Cosentino-Gomes D, Gomes MT, Alviano DS, Alviano CS, Lopes AH, Meyer-Fernandes JR (2011) Biochemical properties of *Candida parapsilosis* ecto-5'-nucleotidase and the possible role of adenosine in macrophage interaction. *FEMS Microbiol Lett* 317:34–42. <https://doi.org/10.1111/j.1574-6968.2011.02216.x>
42. Hamill OP, Marty A, Neher E, Sakmann B, Sigworth FJ (1981) Improved patch-clamp techniques for high-resolution current recording from cells and cell-free membrane patches. *Eur J Physiol* 391:85–100
43. Riccardi C, Nicoletti I (2006) Analysis of apoptosis by propidium iodide staining and flow cytometry. *Nat Protoc* 1:1458–1461. <https://doi.org/10.1038/nprot.2006.238>
44. da Silva-Souza HA, Lira MN, Costa-Junior HM, da Cruz CM, Vasconcelos JS, Mendes AN, Pimenta-Reis G, Alvarez CL, Faccioli LH, Serezani CH, Schachter J, Persechini PM (2014) Inhibitors of the 5-lipoxygenase arachidonic acid pathway induce ATP release and ATP-dependent organic cation transport in macrophages. *Biochim Biophys Acta* 1838:1967–1977. <https://doi.org/10.1016/j.bbame.2014.04.006>
45. Granger DL, Taintor RR, Boockvar KS, Hibbs JB Jr (1996) Measurement of nitrate and nitrite in biological samples using nitrate reductase and Griess reaction. *Methods Enzymol* 268:142–151
46. von Kügelgen I, Hoffmann K (2016) Pharmacology and structure of P2Y receptors. *Neuropharmacology* 104:50–61. <https://doi.org/10.1016/j.neuropharm.2015.10.030>
47. Jacobson KA, Müller CE (2016) Medicinal chemistry of adenosine, P2Y and P2X receptors. *Neuropharmacology* 104:31–49. <https://doi.org/10.1016/j.neuropharm.2015.12.001>
48. Costa-Junior HM, Mendes AN, Davis GHNG, Monteiro-da-Cruz C, Ventura AL, Serezani CH, Faccioli LH, Freire-de-Lima CG, Bisaggio RC, Persechini PM (2009) ATP-induced apoptosis involves a Ca<sup>2+</sup>-independent phospholipase A2 and 5-lipoxygenase in macrophages. *Prostaglandins Other Lipid Mediat* 88:51–61. <https://doi.org/10.1016/j.prostaglandins.2008.09.004>



49. Hu Z, Murakami T, Suzuki K, Tamura H, Kuwahara-Arai K, Iba T, Nagaoka I (2014) Antimicrobial cathelicidin peptide LL-37 inhibits the LPS/ATP-induced pyroptosis of macrophages by dual mechanism. *PLoS One* 9:e85765. <https://doi.org/10.1371/journal.pone.0085765>
50. Keller H, Rentsch P, Hagmann J (2002) Differences in cortical actin structure and dynamics document that different types of blebs are formed by distinct mechanisms. *Exp Cell Res* 277:161–172. <https://doi.org/10.1006/excr.2002.5552>
51. Verhoef PA, Estacion M, Schilling W, Dubyak GR (2003) P2X7 receptor-dependent blebbing and the activation of Rho-effector kinases, caspases, and IL-1 release. *J Immunol* 170:5728–5738. <https://doi.org/10.4049/jimmunol.170.11.5728>
52. Pan Y, Shen B, Gao Q, Zhu J, Dong J, Zhang L, Zhang Y (2016) Caspase-1 inhibition attenuates activation of BV2 microglia induced by LPS-treated RAW 264.7 macrophages. *J Biomed Res* 30:225–233. <https://doi.org/10.7555/JBR.30.20150141>
53. Sperlagh B, Hasko G, Nemeth Z, Vizi ES (1998) ATP released by LPS increases nitric oxide production in raw 264.7 macrophage cell line via P2Z/P2X7 receptors. *Neurochem Int* 33:209–215. [https://doi.org/10.1016/S0197-0186\(98\)00025-4](https://doi.org/10.1016/S0197-0186(98)00025-4)
54. Sakaki H, Tsukimoto M, Harada H, Moriyama Y, Kojima S (2013) Autocrine regulation of macrophage activation via exocytosis of ATP and activation of P2Y11 receptor. *PLoS One* 8:e59778. <https://doi.org/10.1371/journal.pone.0059778>
55. Lévesque SA, Kukulski F, Enjyoji K, Robson SC, Sévigny J (2010) NTPDase1 governs P2X7-dependent functions in murine macrophages. *Eur J Immunol* 40:1473–1485. <https://doi.org/10.1002/eji.200939741>
56. Zanin RF, Braganhol E, Bergamin LS, Campesato LF, Filho AZ, Moreira JC, Morrone FB, Sévigny J, Schetinger MR, de Souza Wyse AT, Battastini AM (2012) Differential macrophage activation alters the expression profile of NTPDase and ecto-5'-nucleotidase. *PLoS One* 7:e31205. <https://doi.org/10.1371/journal.pone.0031205>
57. Wall MJ, Wigmore G, Lopatár J, Frenguelli BG, Dale N (2008) The novel NTPDase inhibitor sodium polyoxotungstate (POM-1) inhibits ATP breakdown but also blocks central synaptic transmission, an action independent of NTPDase inhibition. *Neuropharmacology*:1251–1258. <https://doi.org/10.1016/j.neuropharm.2008.08.005>
58. Van Kolen K, Slegers H (2006) Integration of P2Y receptor-activated signal transduction pathways in G protein-dependent signalling networks. *Purinergic Signal* 2:451–469. <https://doi.org/10.1007/s11302-006-9008-0>
59. Coutinho-Silva R, Ojcius DM, Górecki DC, Persechini PM, Bisaggio RC, Mendes AN, Marks J, Burnstock G, Dunn PM (2005) Multiple P2X and P2Y receptor subtypes in mouse J774, spleen and peritoneal macrophages. *Biochem Pharmacol* 69:641–655. <https://doi.org/10.1016/j.bcp.2004.11.012>
60. da Cruz CM, Ventura AL, Schachter J, Costa-Junior HM, da Silva Souza HA, Gomes FR, Coutinho-Silva R, Ojcius DM, Persechini PM (2006) Activation of ERK1/2 by extracellular nucleotides in macrophages is mediated by multiple P2 receptors independently of P2X7-associated pore or channel formation. *Br J Pharmacol* 147:324–334. <https://doi.org/10.1038/sj.bjp.0706559>
61. Mehta VB, Hart J, Wewers MD (2001) ATP-stimulated release of interleukin (IL)-1 and IL-18 requires priming by lipopolysaccharide and is independent of caspase-1 cleavage. *J Biol Chem* 276:3820–3826. <https://doi.org/10.1074/jbc.M006814200>
62. Miao EA, Rajan JV, Aderem A (2011) Caspase-1-induced pyroptotic cell death. *Immunol Rev* 243:206–214. <https://doi.org/10.1111/j.1600-065X.2011.01044.x>
63. Lamkanfi M, Kalai M, Saelens X, Declercq W, Vandenabeele P (2004) Caspase-1 activates nuclear factor of the kappa-enhancer in B cells independently of its enzymatic activity. *J Biol Chem* 279:24785–24793. <https://doi.org/10.1074/jbc.M400985200>
64. Pan Y, Shen B, Gao Q, Zhu J, Dong J, Zhang L, Zhang Y (2016) Caspase-1 inhibition attenuates activation of BV2 microglia induced by LPS-treated RAW264.7 macrophages. *J Biomed Res* 30:225–233. <https://doi.org/10.7555/JBR.30.20150141>
65. Lee J, Choi J, Kim S (2015) Effective suppression of pro-inflammatory molecules by DHCA via IKK-NF- $\kappa$ B pathway, in vitro and in vivo. *Br J Pharmacol* 172:3353–3369. <https://doi.org/10.1111/bph.13137>
66. Kong Q, Wang M, Liao Z, Camden JM, Yu S, Simonyi A, Sun GY, Gonzalez FA, Erb L, Seye CI, Weisman GA (2005) (2005) P2X7 nucleotide receptors mediate caspase-8/9/3-dependent apoptosis in rat primary cortical neurons. *Purinergic Signal* 1:337–347. <https://doi.org/10.1007/s11302-005-7145-5>
67. Hanley PJ, Kronlage M, Kirschning C, del Rey A, Di Virgilio F, Leipziger J, Chessell IP, Sargin S, Filippov MA, Lindemann O, Mohr S, Königs V, Schillers H, Bähler M, Schwab A (2012) Transient P2X7 receptor activation triggers macrophage death independent of Toll-like receptors 2 and 4, caspase-1, and pannexin-1 proteins. *J Biol Chem* 287:10650–10663. <https://doi.org/10.1074/jbc.M111.332676>
68. Mackenzie AB, Young MT, Adinolfi E, Surprenant A (2005) Pseudoapoptosis induced by brief activation of ATP-gated P2X7 receptors. *J Biol Chem* 280:33968–33976. <https://doi.org/10.1074/jbc.M502705200>
69. Roger S, Pelegrin P, Surprenant A (2008) Facilitation of P2X7 receptor currents and membrane blebbing via constitutive and dynamic calmodulin binding. *J Neurosci* 28:6393–6401. <https://doi.org/10.1523/JNEUROSCI.0696-08.2008>
70. Noronha-Matos JB, Coimbra J, Sá-e-Sousa A, Rocha R, Marinhas J, Freitas R, Guerra-Gomes S, Ferreira F, Costa MA, Correia-de-Sá P (2014) P2X7-induced zeiosis promotes osteogenic differentiation and mineralization of postmenopausal bone marrow-derived mesenchymal stem cells. *FASEB J* 28:5208–5222. <https://doi.org/10.1096/fj.14-257923>
71. Pelegrin P, Surprenant A (2009) The P2X(7) receptor-pannexin connection to dye uptake and IL-1 $\beta$  release. *Purinergic Signal* 5:129–137. <https://doi.org/10.1007/s11302-009-9141-7>
72. Qu Y, Misaghi S, Newton K, Gilmour LL, Louie S, Cupp JE, Dubyak GR, Hackos D, Dixit VM (2011) Pannexin-1 is required for ATP release during apoptosis but not for inflammasome activation. *J Immunol* 186:6553–6561. <https://doi.org/10.4049/jimmunol.1100478>
73. Kayagaki N, Warming S, Lamkanfi M, Vande Walle L, Louie S, Dong J, Newton K, Qu Y, Liu J, Heldens S, Zhang J, Lee WP, Roose-Girma M, Dixit VM (2011) Non-canonical inflammasome activation targets caspase-11. *Nature* 479:117–121. <https://doi.org/10.1038/nature10558>
74. Yang D, He Y, Muñoz-Planillo R, Liu Q, Núñez G (2015) Caspase-11 requires the pannexin-1 channel and the purinergic P2X7 pore to mediate pyroptosis and endotoxemic shock. *Immunity* 43:923–932. <https://doi.org/10.1016/j.immuni.2015.10.009>